Article

JOURNAL OF THE CHINESE CHEMICAL SOCIETY

Physicochemical and Redox Characteristics of Fe Ion-doped CeO_2 Nanoparticles

Anees A. Ansari,[a]* J. Labis,[a] Manawwer Alam,[b] Shahid M. Ramay,[c] Naushad Ahmad[d] and Asif Mahmood[e]

[a]*King Abdullah Institute for Nanotechnology, King Saud University, Riyadh-11451, Saudi Arabia*
[b]*Research Center, College of Science, King Saud University, P.O. Box 2455, Riyadh, Saudi Arabia*
[c]*Department of Physics, King Saud University, P.O. Box 2455, Riyadh, Saudi Arabia*
[d]*Department of Chemistry, College of Science, King Saud University, P.O. Box 2455, Riyadh, Saudi Arabia*
[e]*College of Engineering, Department of Chemical Engineering, King Saud University, Riyadh, Saudi Arabia*

(Received: May 27, 2015; Accepted: Aug. 26, 2015; Published Online: Sept. 18, 2015; DOI: 10.1002/jccs.201500195)

We report the structural, thermal, optical, and redox properties of Fe-doped cerium oxide (CeO_2) nanoparticles, obtained using the polyol-co-precipitation process. X-ray diffraction data reveal the formation of single-phase structurally isomorphous CeO_2. The presence of Fe^{3+} may act as electron acceptor and/or hole donor, facilitating longer lived charge carrier separation in Fe-doped CeO_2 nanoparticles as confirmed by optical band gap energy. The increased content of localized defect states in the ceria gap and corresponding shift of the optical absorption edge towards visible range in Fe-doped samples can significantly improve the optical activity of nanocrystalline ceria. The better-quality redox performances of the Fe-doped CeO_2 nanoparticles, compared with undoped CeO_2 nanoparticles, were ascribed mainly to a decrease in band gap energy and an increase in specific surface area of the material. As observed from TPR studies all Fe -doped CeO_2 nanoparticles, particularly the 10 mol % Fe doped CeO_2 nanoproduct, exhibit excellent reduction performance.

Keywords: Ceria nanoparticles; Optical properties; Band gap energy; Redox properties.

INTRODUCTION

Ceramic materials based on cerium oxide (CeO_2) have been a very active research field due to their applications in various technologies, such as production of oxygen through water decomposition, photo-catalysis devices, corrosion protection, solid oxide fuel cells, humidity/oxygen gas sensor, electrochemical biosensor and as a catalyst in numerous industrial processes.[1-10] Their uses in catalysis are due to their chemical and physical stability, high oxygen mobility at moderate temperature, and high oxygen vacancy concentration. The possibility of switching between reduced and oxidized states (cycling around the redox potential of the Ce^{4+}/Ce^{3+} couple) allows the reversible addition/removal of O_2 to/from CeO_2.[11]

The use of monodispersed nanocrystalline powders as starting materials has demonstrated considerable potential in improving the properties of existing ceramic compositions.[12-14] These noble physical and chemical properties of CeO_2 make them distinguished with other ceramic materials, so that their number of applications has increased rapidly, e.g. glasses, ceramics, phosphors, catalysis, electrochemical biosensors, biotechnology, free radical inhibitor, nano-medicine, and chemical applications, and for which the use of nanocrystalline powders is an important factor.[1-10,15,16] However, the high specific surface areas of nanocrystalline powders, in which the primary particle size is often smaller than 15 nm, also result in a stronger tendency of the powder to agglomerate which can make processing difficult.

To achieve higher specific surface area that is desirable for useful applications, several efforts have been exerted to fabricate nanoporous CeO_2. Liu *et al.* employed different methods to enhance the physicochemical properties of the CeO_2 nanoparticles.[17] Phonthammachai *et al.* used sol-gel chemical process for a preparation of high surface area mesoporous cubic-phase nanocrystalline CeO_2. Masui *et al.* applied micro-emulsion method for preparing ultrafine CeO_2 particles.[19] A nonhydrolytic solution route was utilized for the preparation of highly uniform and well-dispersed CeO_2 and CeO_2:Eu^{3+} (Sm^{3+}, Tb^{3+}) nanocrystals.[20] Tang *et al.* reported CeO_2 nanotubes prepared by controlled annealing of the formed $Ce(OH)_3$ nanotubes.[21] Nanoporous CeO_2 has extremely high surface activity and well oxygen storage capacity due to its porous structure, which can easily absorb various ions in its pores and on its surfaces. Moreover, higher specific surface area and oxy-

* Corresponding author. Tel: +966-1-4676838; Fax: +966-1-4670662; Email: aneesaansari@gmail.com

gen storage capacity as carriers can enhance catalytic activity of catalyst.[4,5,9,10] On the other hand, some alkaline and transition metal ions also have been used as a catalytic promoter in ceria lattice to promote catalytic activity of the ceria nanoparticles.[4,5,22] It is known that noble metal catalysts such as Au which have been frequently studied for CO oxidation have very high catalytic activities.[8,23,24] In addition, other previous reports have shown that the reducibility and catalytic activity of CeO_2 are significantly enhanced by the presence of small amount of transition metal, not in the platinum group.[22] Platinum was the earliest case demonstrating that a metal additive had a considerable effect on ceria reducibility. However, due to the high cost of these noble metals and their sensitivity to sulfur poisoning, more scientists are seeking for new catalysts from the cheaper transition metals, one of which is iron.[25] Recently, doping of some transition metals (e.g., Ni^{2+}, Co^{2+}, and Fe^{2+})[22,25] has been proposed to introduce magnetic functionality in cerium oxide semiconductor. It is reported that lower valence cations (3+) increases the concentration of oxygen vacancies, which are responsible for the high ionic conductivity in CeO_2.[4,5] In the present work, an alternative is explored using Fe^{3+} (instead of Ni^{2+}, Co^{2+}, and Fe^{2+}) as stabilizing additive to ceria, and possess highly defined pore architecture and has very high surface area, thus resulting to a very unique physicochemical properties. Fe^{3+} also has ionic radius smaller than that of Ce^{4+} (so that a stabilization of a small ceria particle size is expected, and indeed, it has been verified for temperatures below 900 °C), but lower than that of M^{2+}, so that incompatibilities with the ceria lattice will be lower and one may thus expect that such a decomposition will not take place. Therefore, physicochemical properties of these Fe^{3+} ions doped CeO_2 are interesting to pursue for their diversified applications.

The present study is aimed to determine the effect of iron doping on physicochemical properties of nanocrystalline ceria synthesized using a wet-chemical synthesis. In this work, we carried out different characterization techniques to investigate the morphological structure, crystalinity, thermal, optical, and temperature program reduction properties of the prepared iron doped ceria nanoparticles. X-ray diffraction pattern and FE-TEM were used to examine the crystalline nature, phase purity and morphology of the doped nanoparticles.

EXPERIMENTAL

Materials and methods: Cerium nitrate (99.99%, BDH Chemicals Ltd, England), ferric nitrate (E-Merck, Germany) ethylene glycol, C_2H_5OH, NH_4OH were used as starting materials without any further purification. Nanopure water was used for the preparation of solutions. The ultrapure de-ionized water was prepared using a Milli-Q system (Millipore, Bedford, MA, USA). All other chemicals used were of reagent grade.

Preparation of Fe ion-doped cerium oxide nanoparticles: In a typical reaction, 0.2M $Ce(NO_3)_3$ $6H_2O$ (98, 95 and 90 mol%) was dissolved in 50 ml ethylene glycol and heated on hot plate upto 80 °C. Separately 0.2M ferric nitrate (2, 5 and 10 mol%) dissolved in ethylene glycol was added drop-wise in the forgoing reaction and whole solution is kept under magnetic stirring on hotplate at 80 °C to obtain homogenous mixture. Later this homogenously mixed solution was transfered in a 250 ml round bottle flask fitted with reflux condenser and hydrolyzed for 24 h. A required amount of ammonia was added to the hydrolyzed solution and the precipitate was obtained. The obtained gray colored precipitate was centrifuged and washed several times with distilled water to remove excess amount of ammonium and nitrate ions and dried the obtained product at 100 °C. The prepared samples were annealed at 400 °C in air for 2 h. We have examined systematic changes in the color of the cerium hydroxide precipitate. The color of the prepared cerium hydroxide precipitate has changed gradually from gray to yellow after being exposed to air. This could be due to the oxidation of peroxide $Ce(OH)_3OOH$ to $Ce(OH)_4$ by oxygen. This procedure was repeated for the synthesis and purification of different Fe-doped CeO_2 concentrations.

Characterization: The crystalinity of the powder samples were examined by X-ray diffraction (XRD) at room temperature with the use of Rigaku- Dmax 2500 diffractometer equipped with Cu K_α (λ = 1.54056 Å) radiations as X-ray source. Thermogravimetric analysis (TGA) was performed with TGA/DTA, Mettler Toledo AG, Analytical CH-8603, Schwerzenbach, Switzerland. The size and morphology of the samples were inspected using a field emission transmission electron microscope (FE-TEM) equipped with the EDX (FETEM, JEM-2100F, JEOL, Japan) operating at an accelerating voltage of 200 kV. EDX analysis was used to confirm the presence of the elements. The samples for TEM were prepared by depositing a drop of a colloidal ethanol solution of the powder sample onto a carbon-coated copper grid. The FTIR spectra were recorded on a Perkin-Elmer 580B IR spectrometer using KBr pellet technique in the range 4000-400 cm^{-1}. The UV/Vis absorption spectra were measured in the Perkin-Elmer Lambda-40 spectrophotometer in the range 200–600 nm, with the sample contained in 1 cm^3 stoppered quartz cell of 1 cm path length. All measurements were performed at room tempera-

ture. Temperature-programmed reduction (TPR) profiles were obtained using the Micromeritics Autochem model 2910 instrument. The samples were pretreated with high-purity (99.98%) argon (20 ml/min) at 773K for 3 h. After cooling to ambient temperature, the argon atmosphere was replaced by a 5% H_2 in argon mixture, and the catalyst was heated to 873K at a rate of 5 K/min. The flow rate of the H_2–Ar mixture used for this purpose was 40 ml/min. The water produced during the reduction step was condensed and collected in a cold trap immersed in the slurry of an isopropanol–liquid nitrogen mixture.

RESULTS AND DISCUSSION

Crystal structure, phase purity and particle size

XRD characterization was performed to study the crystal structure and phase purity of the as-synthesized Ferric ion doped cerium oxide nanoparticles. As shown in Figure 1, all diffraction peaks such as (111), (200), (220), (311) and (222) planes, are well indexed to the single-phase fluorite cubic structure of CeO_2 (space group: *Fm3m*) with lattice constant a = 5.411 Å. This is in good agreement with the JCPDS file for CeO_2 (JCPDS 34–0394).[20,26-28] No other potential impurities of iron oxide such as (Fe_2O_3, $FeCeO_3$, and $FeCe_2O_4$) can be observed from the XRD patterns over the entire doping range. The broadening of the peaks indicates that the crystallite sizes are neutrally small (14.5-13.3 nm). It is observed from Fig. 1 that the widths of all peaks were broad indicating nanocrystalline sizes.[20,26-28] The calculated average grain size estimated from the Debye-Scherrer formula for (a) 14.5 nm for 2 mol%, 13.4 nm for 5 mol% and 13.3 nm for 10 mol% of Ferric ion doped CeO_2 nanoparticles. The calculated lattice parameter using the XRD patterns for the obtained products are found to be (a) 5.4007 (b) 5.3907 (c) 5.3923 Å, respectively, which are slightly lower than its bulk counterpart (5.411 Å). From the XRD patterns we observed that both particle size as well as lattice parameters sharply decreases with increasing Fe-doping concentration in CeO_2 nanoparticles compared to the bulk counterpart. The lowering of the lattice parameter of the as-prepared sample may be attributed to the fact that during crystallization by annealing, Fe-ions with relatively lower atomic size compared to that of Ce-ions have entered and settled in the CeO_2 lattice. Moreover, it can be noted that doping CeO_2 with Fe^{3+} can also hinder grain growth as well. This supports the decreasing crystallite sizes reported elsewhere.[28-30] These results are in good agreement with the earlier reports on the transition metal doped CeO_2 nanoparticles.[22,31] Recently, Thuber *et al*. reported a similar result on transition metal ion-doped CeO_2 nanoparticles. They observed that lattice strain decrease up to the 4% doping of Ni ions and found to increase with further doping of Ni ions.[32] They explained that the decrease in the lattice strain is due to the replacement of Ce by Fe ions in the host matrix and the increase in the lattice strain above 4% doping is due to the interstitial incorporation of Fe ions. However, in the present case, we have observed that lattice strain decreases from 3.08×10^{-3} to 1.96×10^{-3} with Fe doping up to 10%. This observed behavior of particle size, lattice parameters and lattice strain indicates the all Fe ions could have replaced Ce ions in the CeO_2 host matrix. Moreover, the peak intensity of (111) plane decreases with increasing Fe-dopant concentration. This implies that the increasing incorporation of Fe ions unto the CeO_2 lattice tends to lower the crystallinity of the latter due to introduction of a harmonicities in the lattice by the foreign cation. As the peaks in the XRD patterns are normally broad and wide in nanocrystalline system, therefore it is difficult to resolve the closely spaced peaks separately. Thus, the possibility of formation of the α-Fe_2O_3 phase cannot be simply ruled out by XRD alone. However, no characteristic reflection of γ-Fe_2O_3 has yet been observed.

Morphological structure

The size and morphology of the prepared Fe-doped CeO_2 nanoparticles are analyzed by TEM. Fig. 2 shows the typical images of as-prepared nanopowders and reveals that hydrothermal-co-precipitation products consist of well

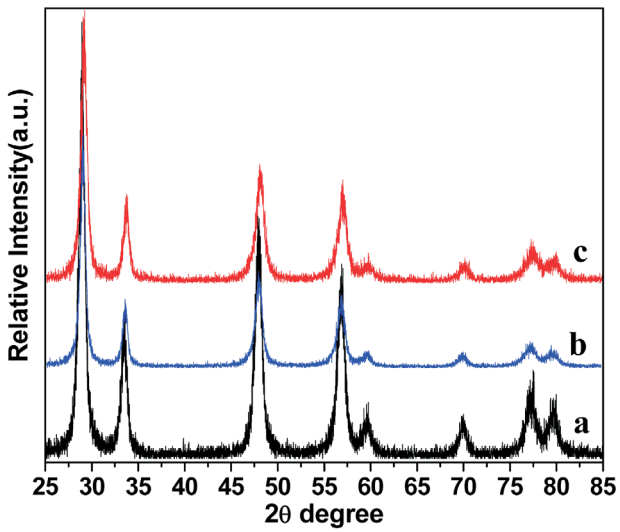

Fig. 1. X-ray diffraction pattern of (a) CeO_2:Fe2% (b) CeO_2:Fe5% and (c) CeO_2: Fe10% nanoparticles.

dispersed quasi-spherical nanoparticles with diameters in the range of 10-15 nm. TEM micrographs show that the prepared nanocrystals are in irregular shapes and sizes, and are highly aggregated with a narrow size distribution. The average crystalline sizes are quite close to the particle size obtained from XRD patterns. This consistency suggests that individual particles obtained are nanocrystallites. The inset in Fig. 2a-c show the electron diffraction pattern (SAED) for the Fe-doped CeO_2 nanoparticles, indicating the polycrystalline nature of the nanoproducts. These results complement the XRD patterns. The calculated interplanar distance between the adjacent lattice fringes is in good agreement with the (111) spacing of the standard value (0.352 nm) and lattice planes of cubic fluorite structure CeO_2 (JCPDS no. 17-0341). The EDX was also performed on the synthesized nanoparticles. It is observed that the cerium (Ce), Ferric (Fe) and oxygen (O) atoms are well-distributed inside the nanoparticle in all samples. From Fig. 3a-c, the peak of Fe increases gradually from sample a to c due to the increase in iron doping. Note that the C and Cu signals were from the TEM Cu grid (substrate).

Thermogravimatric analysis

Thermal stability of the synthesized Fe-doped CeO_2

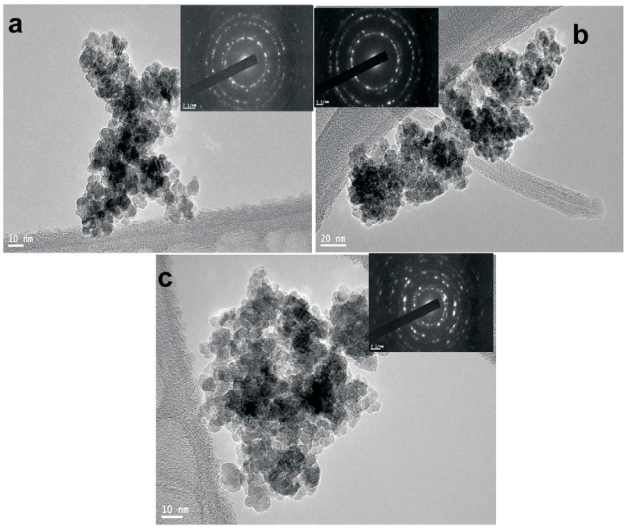

Fig. 2. FE-TEM micrographs of the as-prepared (a) CeO_2:Fe2% (b) CeO_2:Fe5% and (c) CeO_2: Fe10% nanoparticles and inset of the images show the selected area electron diffraction pattern.

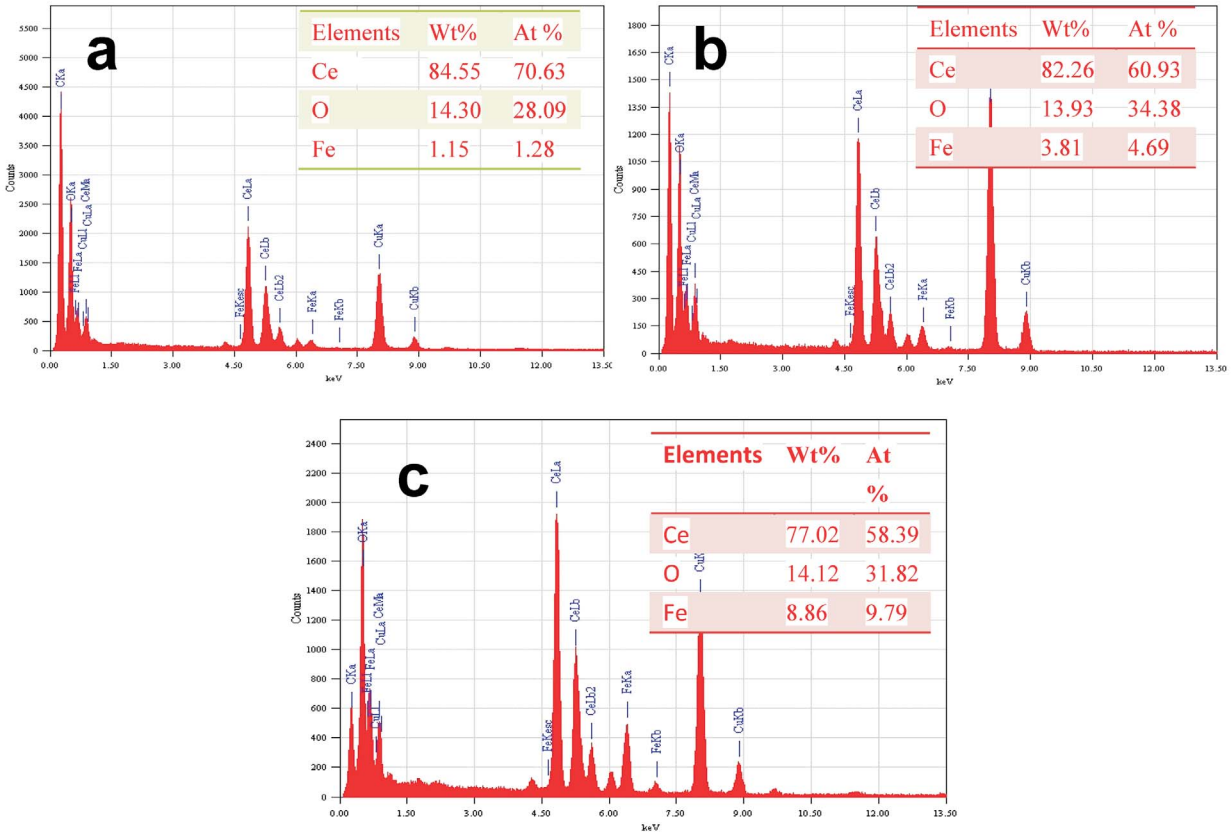

Fig. 3. EDX analysis of the as-prepared (a) CeO_2:Fe2% (b) CeO_2:Fe5% and (c) CeO_2: Fe10% nanoparticles.

nanoparticles was determined by thermo-gravimetric analysis between ambient to 800 °C under N_2 atmosphere at a heating rate of ~10 °C/min (Fig. 4a-c). All thermograms show similar decomposition trend in two steps. In the first step, the TGA indicated a minor weight loss (around ~2%) between 25-200 °C. This is due to physically absorbed water molecules around the surface of doped metal oxide nanoparticles. In the second step, all thermograms reveal a sluggish weight loss (~4%) between 200 and 800 °C, which is due to the removal of small amount of dangling bonds present on the surface of the nanoparticles. After 800 °C, no obvious weight loss was observed. The thermograms have confirmed the phase purity of the as-synthesized nanoparticles in accord with the XRD results.

Optical characteristics

Fig. 5 illustrates the FTIR spectra of the prepared Fe-doped CeO_2 nanoparticles. All spectra exhibit a broad band around 3445 cm^{-1}, due to the O-H stretching vibration of physically absorbed water molecules on the surface of nanoparticles.[33] Two weak bands in the spectra of Fe-doped CeO_2 nanoparticles at 1622 and 1408 cm^{-1} are also observed, which are ascribed to the bending mode of Ce-O-H groups. This correlates with the TGA results. Another strong infrared band was also observed below 600 cm^{-1} which is due to the presence of asymmetric bending vibrations involved in the Ce-O-Fe network.[33]

UV-Vis spectroscopy was employed to characterize the optical features of the prepared-doped CeO_2 nanoparticles at different iron concentration. As shown in Fig. 6, the absorption spectra display broad absorption band centered at around 328 nm, originating from charge transfer transition between 2p orbital of O and 4f orbital of Ce^{4+} in CeO_2. These spectral results agree well with the previous observations (Fig. 6).[27,34] For all samples, the absorbance dispersions have the same general shape that is monotonically increasing with increasing photon energy. However, they have slight difference in the magnitude, slope of the curves in the linear regions, and the photon energy at which nanoparticles begin to absorb strongly.

The band gap can be determined by fitting the absorption data to the direct transition equation by extrapolating

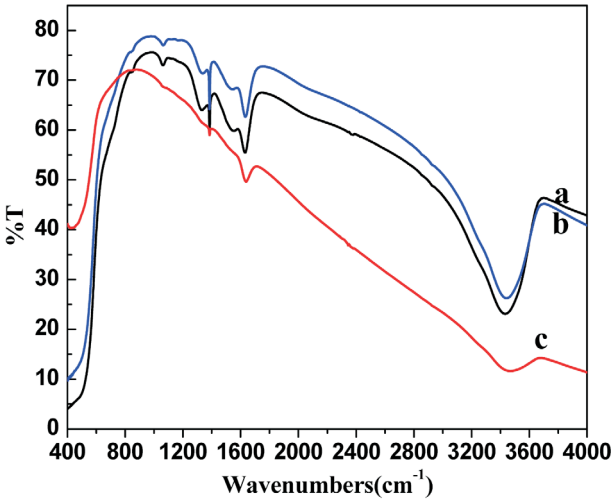

Fig. 5. FTIR spectra of the as-prepared (a) CeO_2:Fe2% (b) CeO_2:Fe5% and (c) CeO_2: Fe10% nanoparticles.

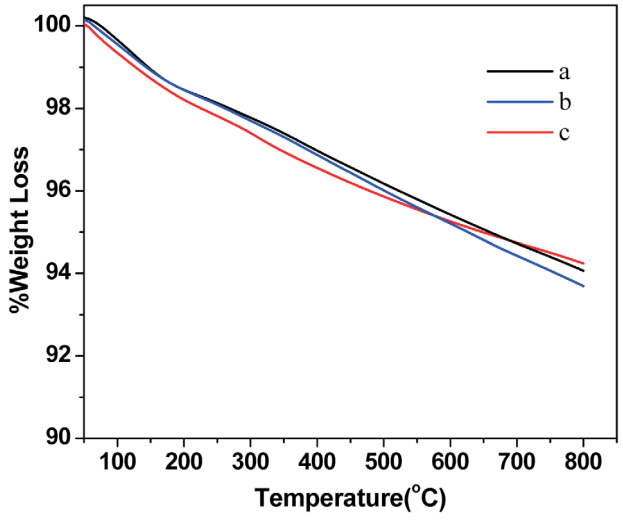

Fig. 4. Thermo-gravimetric analysis of (a) CeO_2:Fe2% (b) CeO_2:Fe5% and (c) CeO_2: Fe10% nanoparticles.

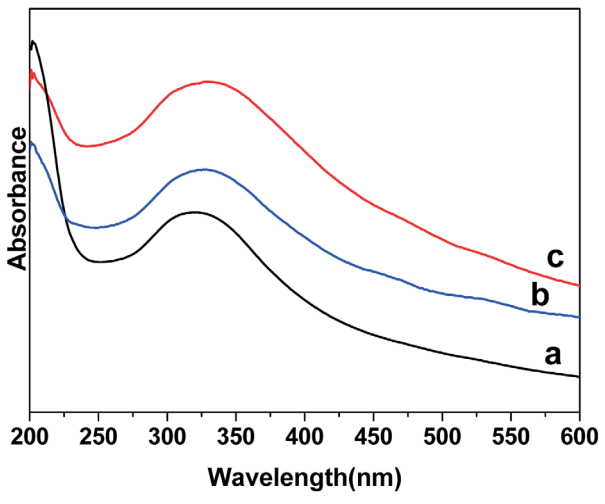

Fig. 6. UV-vis absorption spectra of (a) CeO_2:Fe2% (b) CeO_2:Fe5% and (c) CeO_2: Fe10% nanoparticles suspended in ethanol.

the linear portions of the curves to absorption to zero (Fig. 7)

$$\alpha h\nu = E_D (h\nu - E_g)^{1/2}$$

where α is the optical absorption coefficient, $h\nu$ is the photon energy, E_g is the direct band gap, and ED is a constant. The correlated band gaps are 2.35, 2.03, and 1.90 eV corresponding to 2, 5 and 10 mol% Fe^{3+} doping, respectively.[19,20,27,34] Xia *et al.* speculated that the peak shift was the result of the defects (such as oxygen vacancies) or the impurities caused from the incorporation of the transition metal ions as the defects and impurities could result in the formation of sublevels within the band gap.[35] In conclusion, the increase or decrease in band-gap can be interpreted as follows. As the doping concentration in semiconductors increases, the Fermi level which initially lies between the conduction band and donor energy level begins to enter the conduction band. This shift decreases with increase in doping. This implies that there is an decrease in the optical band-gap. This effect is called Moss–Burstein effect.[36] Beyond 2% Fe^{3+} doping, the interactions between the electron–electron, electron–donor atoms, and electron–hole increase drastically resulted in the decrease in band-gap.[37]

TPR studies

The TPR experiments using H_2 were performed to analyze the redox properties of iron doped ceria samples calcined at 500 °C. The corresponding TPR profiles are shown in Fig. 8. The ceria shows two typical characteristic reduction peaks; the low temperature peak (~124 °C) is assigned to the easily reducible surface capping oxygen, whereas the high temperature peak (at ~402 °C and not shown in the figure) is due to the removal of bulk oxygen. The incorporation of iron into the ceria lattice strongly modified the reduction behavior of ceria by shifting surface and bulk reduction to lower temperatures. For 2, 5 and 10 mol%, Fe-doped ceria samples calcined at 500 °C, the corresponding temperatures are 350, 357 and 347 °C, respectively. It is interesting to note that the reduction temperature for the 10 mol%, –doped ceria sample was lower compared to the 2 mol%. One possible reason for this behavior is the enhancement of oxygen vacancies (as supported from previous XRD patterns) which increases the oxygen mobility in the lattice.[26,28] Moreover, it is known that iron addition induces ordered arrangements of vacancies, thereby creating a pathway for oxygen diffusion. This would promote oxygen ion diffusion from the bulk to the surface enabling the bulk reduction at low temperatures. The oxygen storage/release property of ceria is the most important factor which contributes to the catalytic activity of ceria in oxidation reactions.[5] Clearly, the H_2-TPR results demonstrate that there is a strong synergistic interaction between iron and cerium species that facilitates reduction of both iron and cerium. As the doping content of iron is increased into the ceria lattice leading to higher H_2 consumption, it does not show any additional peak of iron in all samples. Notably, the H_2 uptake for the 2, 5 and 10 mol%, Fe-doped ceria samples is 0.024, 0.056 and 0.0594, respectively, suggesting that the catalysts become more reducible with lower aging temperature. Moreover, it is found that the excess hy-

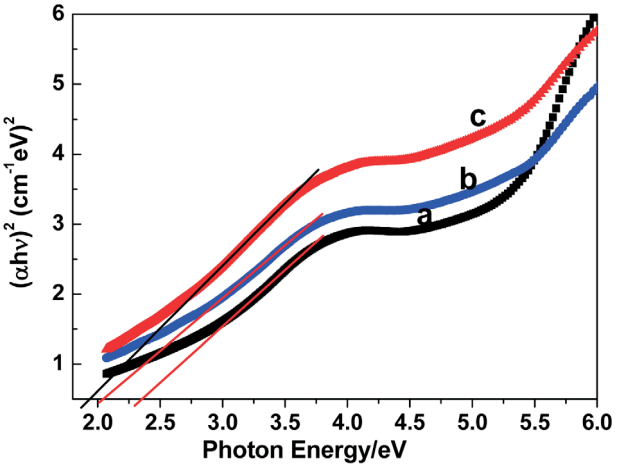

Fig. 7. Plot of $(\alpha h\upsilon)^2$ vs. photon energy (h) of the (a) CeO_2:Fe2% (b) CeO_2:Fe5% and (c) CeO_2:Fe10% nanoparticles.

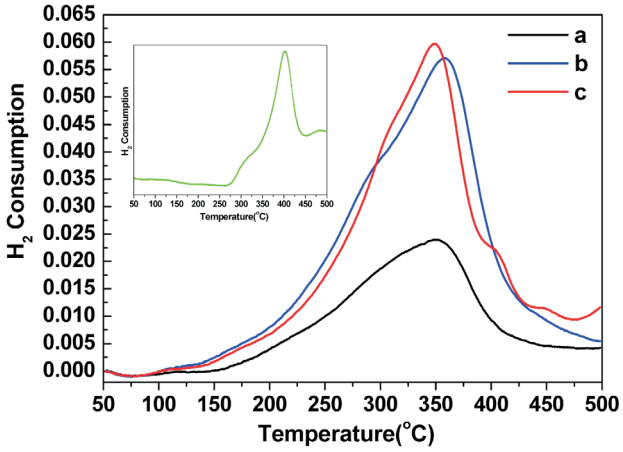

Fig. 8. H_2-TPR profiles of (a) CeO_2:Fe2% (b) CeO_2:Fe5% and (c) CeO_2:Fe10% nanoparticles, inset shows the TPR result of pure CeO_2.

drogen are consumed for10 mol%, Fe-doped ceria sample. This means that the CeO_2 is reduced simultaneously with the reduction of Fe_2O_3 to Fe_3O_4, which is due to the metal–support strong interaction and thus promotes the reduction of ceria. Previous reports[25,38] showed that the presence of iron would weaken the Ce–O bond adjacent to iron species and facilitate reducibility of surface-capping oxygen of ceria. Therefore, the peaks with maxima at about 350 °C, for Fe-doped CeO_2 nanoparticles, can be due to the reduction of surface-capping oxygen of CeO_2 interact with iron.[25,38] Therefore, these results show that both the composition and textural parameters of the catalysts have pronounced effects on their reducibilities. In addition, other effects such as differences in iron dispersion in CeO_2, oxygen vacancies, photoluminescence and Raman spectroscopy which give vibrational structure of the ceria lattice could have contributed to this effect but still under investigations.[38,39] Further, oxygen vacancies are also believed to have played an important role in CO oxidation and can be considered as an indicator for the promotion of the reaction.

CONCLUSIONS

Nanocrystalline Fe(III)-doped CeO_2 powder were synthesized from the reaction of $Ce(NO_3)_36H_2O$ (0.98, 0.95 and 0.90 mol%) and $Fe(NO_3)_3xH_2O$ (0.02, 0.05 and 0.10 mol%) through polyol assisted co-precipitation process, which provides a convenient one-step, low-cost, nontoxic, and mass-production route. The oxidation of CeO_2 from trivalent to tetravalent is compensated by oxygen vacancies, which can cause distortion of the crystal lattice affecting the physical, chemical and optical properties of the final product. The possibility to modulate the Ce^{3+}/Ce^{4+} content and particle sizes depending on the doping concentrations, is interesting for applications in the catalysis and optical fields. Owing to the defects and impurities, the absorption spectra of the CeO_2 show that the peak shifts from the ultraviolet region to the visible light region after being doped with Fe ions. Our results indicate that the band gap energies were affected as the doping contents increases due to the quantum confinement effect. The experimental results on temperature program reduction showed that Fe ion enhances the reduction of CeO_2 (reduced low temperature ~350 °C) compared with that of the pure CeO_2 nanoproduct (~405 °C). Enhancement of the reduction temperature of CeO_2 nanoparticles upon Fe doping may be due to an increase in the charge transport rate. The thermal stability and ability to release a substantial amount of oxygen at relatively low temperatures makes the Fe doped CeO_2 nanoparticles a potential material for oxygen storage/release and automotive catalytic applications.

ACKNOWLEDGEMENT

The authors extend their sincere appreciations to the Deanship of Scientific Research at King Saud University for its funding this Prolific Research group (PRG-1436-26).

REFERENCES

1. Ansari, A. A.; Solanki, P. R.; Malhotra, B. D. *App. Phys. Lett*. **2008**, *93*, 263901.
2. Ansari, A. A.; Solanki, P. R.; Malhotra, B. D. *J. Biotechnol.* **2009**, *142*, 179.
3. Liao, L.; Mai, H. X.; Yuan, Q.; Lu, H. B.; Li, J. C.; Liu, C.; Yan, C. H.; Shen, Z. X.; Yu, T. *J. Phys. Chem. C* **2008**, *112*, 9061.
4. Yen, H.; Seo, Y.; Kaliaguine, S.; Kleitz, F. *Angew. Chem. Int. Ed*. **2012**, *51*, 12032.
5. Mahammadunnisa, S.; Reddy, P. M. K.; Lingaiah, N.; Subrahmanyam, C. *Catal. Sci. Technol.* **2013**, *3*, 730.
6. Banerjee, S.; Devi, P. S.; Topwal, D.; Mandal, S.; Menon, K. *Adv. Funct. Mater.* **2007**, *17*, 2847.
7. Robert, C. L.; Long, J. W.; Pettigrew, K. A.; Stroud, R. M.; Rolison, D. R. *Adv. Mater.* **2007**, *19*, 1734.
8. Yu, T.; Zeng, J.; Lim, B.; Xia, Y. *Adv. Mater.* **2010**, *22*, 5188.
9. Si, R.; Zhang, Y. W.; You, L. P.; Yan, C. H. *Angew. Chem. Int. Ed.* **2005**, *44*, 3256.
10. Yu, T.; Joo, J.; Park, Y. I.; Hyeon, T. *Angew. Chem. Int. Ed.* **2005**, *44*, 7411.
11. Deshpande, S.; Patil, S.; Kuchibhatla, S. V. N. T.; Seal, S. *Appl. Phys. Lett*. **2005**, *87*, 133113.
12. Chen, H. I.; Chang, H. Y. *Ceram. Intern*. **2005**, *31*, 795.
13. Miaoa, J. J.; Wanga, H.; Lia, Y. R.; Zhu, J. M.; Zhu, J. J. *J. Crys. Growth* **2005**, *281*, 525.
14. Zhang, D. E.; Zhang, X. J.; Ni, X. M.; Song, J. M.; Zheng, H. G. *ChemPhysChem* **2006**, *7*, 2468.
15. Chen, J.; Pati, S.; Seal, S.; McGinnis, J. F. *Nat. Nanotechnol.* **2006**, *1*, 142.
16. Colon, J.; Herrera, L.; Smith, J.; Patil, S.; Komanski, C.; Kupelian, P.; Seal, S.; Jenkins, D. W.; Baker, C. H. *Nanomed. Nanotech. Biol. Med*. **2009**, *5*, 225.
17. Li, M.; Liu, Z.; Hu, Y.; Shi, Z.; Li, H. *Coll. Surf. A-Physicochem. Eng. Asp.* **2007**, *301*, 153.
18. Phonthammachai, N.; Rumruangwong, M.; Gulari, E.; Jamieson, A. M.; Jitkarnka, S.; Wongkasemjit, S. *Coll. Surf. A-Physicochem. Eng. Asp.* **2004**, *247*, 61.
19. Masui, T.; Fujiwara, K.; Machida, K.; Adachi, G. *Chem. Mater.* **1997**, *9*, 2197.
20. Wang, Z.; Quan, Z.; Lin, J. *Inorg. Chem.* **2007**, *46*, 5237.

21. Tang, C.; Bando, Y.; Liu, B.; Golberg, D. *Adv. Mater.* **2005**, *17*, 3005.
22. Zhang, J.; Guo, J.; Liu, W.; Wang, S.; Xie, A.; Liu, X.; Wang, J.; Yang, Y. *Eur. J. Inorg. Chem.* **2015**, *2015*, 969.
23. Fu, Q.; Deng, W.; Saltsburg, H.; Stephanopoulos, M. F. *Appl. Catal. B: Environ*. **2005**, *56*, 57.
24. Qu, Z.; Yu, F.; Zhang, X.; Wang, Y.; Gao, J. *Chem. Eng. J.* **2013**, *229*, 522.
25. Channei, D.; Inceesungvorn, B.; Wetchakun, N.; Ukritnukun, S.; Nattestad, A.; Chen, J.; Phanichphant, S. *Sci. Rep.* **2014**, *4*, 5757.
26. Babu, S.; Schulte, A.; Seal, S. *Appl. Phys. Lett*. **2008**, *92*, 123112.
27. Ansari, A. A. *J. Semicond.* **2010**, *31*, 053001.
28. Patil, S.; Seal, S.; Guo, Y.; Schulte, A.; Norwood, J. *Appl. Phys. Lett*. **2006**, *88*, 243110.
29. Azam, A.; Ahmed, A. S.; Chaman, M.; Naqvi, A. H. *J. Appl. Phys*. **2010**, *108*, 094329.
30. Tiana, Z. M.; Yuan, S. L.; Hea, J. H.; Lia, P.; Zhanga, S. Q.; Wanga, C. H.; Wanga, Y. Q.; Yina, S. Y.; Liu, L. *J. Alloys Comp*. **2008**, *466*, 26.
31. Channeia, D.; Inceesungvorn, B.; Wetchakun, N.; Phanichphant, S.; Nakaruk, A.; Koshy, P.; Sorrell, C. C. *Ceram. Intern*. **2013**, *39*, 3129.
32. Thurber, A.; Reddy, K. M.; Shutthanandan, V.; Engelhard, M. H.; Wang, C.; Hays, J.; Punnoose, A. *Phys. Rev. B* **2007**, *76*, 165206.
33. Ansari, A. A.; Kaushik, A.; Solanki, P. R.; Malhotra, B. D. *Electrochem. Commun*. **2008**, *10*, 1246.
34. Ansari, A. A.; Singh, S. P.; Malhotra, B. D. *J. Alloy Comp.* **2011**, *509*, 262.
35. Xia, C. H.; Hu, C. G.; Chen, P.; Wan, B. Y.; He, X. S.; Tian, Y. H. *Mater. Res. Bull*. **2010**, *45*, 794.
36. Hao, Y. M.; Lou, S. H.; Zhou, S. M.; Yuan, R. J.; Zhu, G. Y.; Li, N. *Nanoscale Res. Lett.* **2012**, *7*, 1–9.
37. Overstraeten, R. J. V.; Mertens, R. P. *Solid State Electron*. **1987**, *30*, 1077.
38. Brito, P. C. A.; Santos, D. A. A.; Duque, J. G. S.; Macedo, M. A. *Phys. B* **2010**, *405*, 1821.
39. Mitrovic, Z. D. D.; Radovic, M.; Scepanovic, M.; Brojcin, M. G.; Popovic, Z. V.; Matovic, B.; Boskovic, S. *Appl. Phys. Lett.* **2007**, *91*, 203118.

